# Filter-based Pose Estimation for Electric Vehicles Relative to a Ground-based Charging Platform Using On-board Camera Images

ALEXANDER HANEL[1], PRAJWALA SUDI[2], STEPHAN PFENNINGER[2], ECKEHARD STEINBACH[3] & UWE STILLA[1]

*Abstract: Efficient inductive charging of electric vehicles requires the accurate alignment of the vehicle above a ground-based inductive charging platform. This can be achieved using on-board cameras observing the charging platform during the approach manoeuvre. In this contribution, a method for vehicle pose estimation relative to the charging platform is proposed. Vehicle dynamics data obtained from independent pose estimates relying on either markers or markerless features are fused by Kalman filtering to mutual vehicle pose estimates, wherefore the method can be used even when the vehicle is close to the charging platform and the markers are no longer visible in the on-board camera images. The method has been tested with simulated data along trajectories of typical approach manoeuvers to parking lots with a charging platform at the end of the trajectories. Independent from the vehicle motion model and the tested trajectory, deviations of estimated positions from the ground truth of around 0.5 m at the charging platform have been achieved when using dynamics data from both independent pose estimates with an extended Kalman filter.*

## 1 Inductive charging of electric vehicles at charging platforms

Development of electro mobility leads to new requirements for vehicles and external infrastructure. Among these requirements, supplying power to the vehicles plays an important role. Nowadays, plug-in electric vehicles carry a battery providing energy to one or more electrical engines. Typically, batteries of such vehicles are charged using a wired connection between the vehicle and a power socket at a charging station. Alternatives to wired connections are exchanging the battery at battery swapping stations (either stationary or mobile) (SHAO et al. 2017) or doing inductive charging (HWANG et al. 2016). With inductive charging, townscapes don't get changed by many charging stations along the streets and charging becomes more comfortable for the drivers of electric vehicles, to mention just two advantages. Power can be supplied via inductive charging both if the vehicles are being driven or being parked. In both cases, vehicles and roads or parking lots have to be equipped with electromagnetic coils for the power transfer to the vehicle. According to PANCHAL et al. (2018), two aspects have strong negative influence on the efficiency of the inductive charging process of electric vehicles: A large air-gap (ground clearance of vehicles) and misalignment between the coils at the vehicle and in the roads or parking lots. Methods for reducing

---

[1] Technical University of Munich, Photogrammetry & Remote Sensing, Arcisstraße 21, D-80333 Munich, E-Mail: [alexander.hanel, stilla]@tum.de

[2] ServiceXpert Gesellschaft für Service-Informationssysteme mbH, Wandsbeker Allee 77, D-22041 Hamburg, E-Mail: [prajwala.sudi, stephan.pfenninger]@servicexpert.de

[3] Technical University of Munich, Chair of Media Technology, Arcisstraße 21, D-80333 Munich, E-Mail: eckehard.steinbach@tum.de

the air-gap to increase the efficiency are often limited, for example to vehicles with adaptive air suspension. In contrast, the degree of misalignment can be reduced by placing the vehicle accurately above the coils. Accurate placement can be realized especially for inductive charging platforms installed in parking lots, where specific approach manoeuvres can be driven. When approaching the platform with the vehicle, the induced voltage can be used up to a maximal misalignment of around 60 cm (induced voltage has almost reached zero) as a measure for fine alignment (HWANG et al. 2016). Coarse alignment enabling a smooth approach manoeuvre requires therefore a different method. One possibility would be to use the vehicle position obtained by GPS to determine the relative pose to the charging platform and to guide the vehicle closer to the charging platform. This approach is not always practical as for example in dense urban areas with limited space vehicles are often parked in parking garages, where typically no GPS signal is available. For such situations, a possibility would be to detect the charging platform in images acquired by an environment-observing optical on-board camera in the vehicle during the approach manoeuvre and to derive the relative pose between vehicle and charging platform. Compared to other typical environment-observing sensors in vehicles like LiDAR or radar, optical cameras are relatively cheap (e.g. BMW parts catalogue, e.g. available at BMWFANS.INFO 2017) and mounted at several places of a car providing a good overview over the environment around the car on different sides (e.g. ZIEBINSKI et al. 2016). Among all cameras, front-looking ones are considered as most important for this task, as they observe the upcoming driveway.

For both autonomously-driven cars relying on cameras for environment perception and human drivers, modern charging platforms installed completely below the road surface (e.g. Bombardier primove, BOMBARDIER TRANSPORTATION 2013), could be made visible for example by special markers attached to the ground. Common markers for photogrammetric applications, e.g. for vehicle geometry inspection (AICON 3D SYSTEMS GMBH 2018), are circular markers (e.g. described by NAIMARK & FOXLIN 2002) providing one reference point per marker. Other markers, like the squared ArUco markers (ROMERO RAMIREZ et al. 2018), provide four reference points per marker, one per corner. Reference points with known 3D object coordinates and corresponding 2D image coordinates allow estimating the camera pose relative to the markers by solving the perspective-n-point problem, for example. In the case markers are representing a charging platform, the relative pose between the camera-carrying vehicle and the platform can be obtained.

Regardless of the camera position at the vehicle, markers attached to the ground will become invisible in images when the vehicle is close to the platform. In such situations, marker-based pose estimation becomes impossible. Nevertheless, algorithms like structure-from-motion (e.g. FITZGIBBON & ZISSERMAN 1998), visual SLAM (e.g. LEMAIRE et al. 2007) or visual odometry (e.g. NISTER et al. 2004) allow for vehicle pose estimation also in such situations (HANEL & STILLA 2017). Therefore, typically markerless image features like SIFT (LOWE 1999), SURF (BAY et al. 2008) or ORB (RUBLEE et al. 2011) are used to obtain matches between images and to create a map of the environment around the vehicle. Consequently, pose estimation becomes possible for images taken in mapped parts of the environment. However, estimated poses are not directly related to the charging platform.

In this paper, a method for iteratively estimating the vehicle pose during an approach manoeuvre to a charging platform using images from a front-looking on-board camera is proposed, which can

be used for both cases that markers representing the charging platform can be detected in the acquired images or not. The key contribution of this paper is the evaluation of the performance of the proposed method for different vehicle motion models, for the cases that special markers have been detected or not and for different filtering methods for data fusion between poses obtained using markers and poses obtained without seeing markers on simulated data of trajectories of typical parking manoeuvers.

## 2 Method for vehicle pose estimation during approach manoeuvres to a charging platform

Objective of the method proposed in this paper is to estimate the vehicle pose relative to a charging platform iteratively during an approach manoeuvre to the platform using images taken with a front-looking on-board camera. It is assumed that the charging platform is located in a parking lot of a parking garage or another place, where the beginning of the approach manoeuvre is known, for example by the known entry point to the parking garage. It is further assumed that the charging platform is represented by special markers attached to the ground, which can be detected in images and used for estimating the vehicle pose. By fusing vehicle dynamics data (e.g. vehicle position or vehicle velocity, depending on the dynamics model) obtained independently by pose estimation using special markers with vehicle dynamics data obtained by pose estimation using image features, the proposed method allows to estimate the vehicle pose even when the vehicle is close to the charging platform and the markers are not visible in the camera images.

The algorithm for pose estimation consists of the following two steps, which are supposed to be performed iteratively for every image $i$ acquired with the on-board camera during an approach manoeuvre. In the first step, depending on whether a sufficient number of markers has been detected, either stage 1 or stage 2 is performed for obtaining vehicle dynamics data: Stage 1 (Fig. 1, sufficient number of markers detected): Vehicle position estimates $x_i$ and $y_i$ are obtained as vehicle dynamics data from pose estimation using markers on the charging platform ("MB method"). Independently, vehicle velocity estimates $v_{x_i}$ and $v_{y_i}$ are obtained as dynamics data from pose estimation using a markerless method like SLAM or structure-from-motion ("ML method") relying on image features. Stage 2 (Fig. 2, not sufficient number of markers detected): No position estimates are obtained by the MB method as no markers are visible, vehicle velocity estimates are
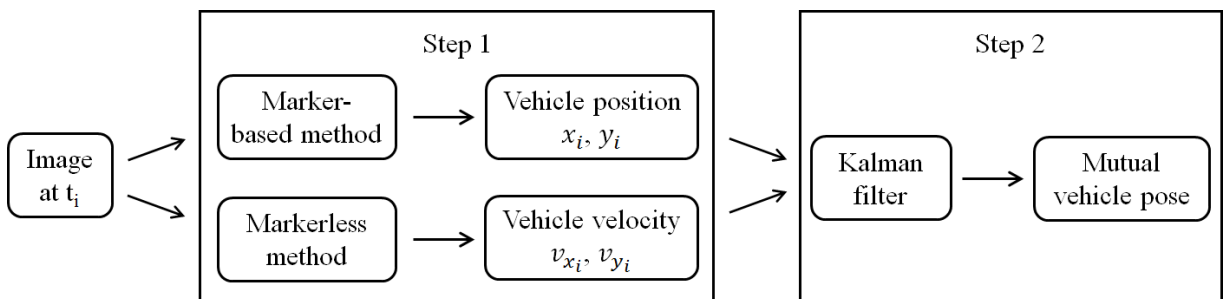


Fig. 1: Stage one workflow for vehicle pose estimation with markers and markerless image features assuming that the charging platform is visible in the acquired on-board camera images.

obtained by the ML method as in stage 1. In the second step, mutual vehicle pose estimates according to a vehicle motion model describing vehicle dynamics are obtained by fusing available position and velocity estimates using a Kalman filter.
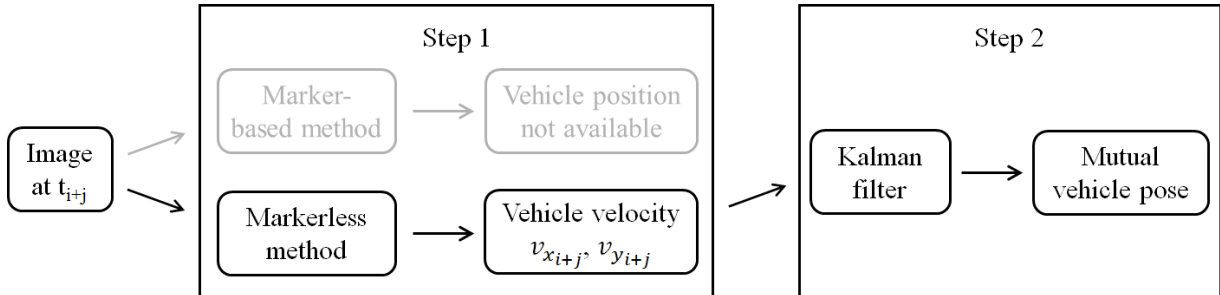


Fig. 2: Stage two workflow for vehicle pose estimation with markerless image features only assuming that the charging platform is not visible in the acquired on-board camera images.

## 2.1 Marker-based vehicle pose estimation ("MB method")

Marker-based estimation of vehicle poses relies on reference points provided by special markers representing the charging platform. The vehicle dynamics data $x_i$ and $y_i$ describing the planar vehicle position are obtained from pose estimation and are fed to the Kalman filter as measurement at time point $t_i$.

Many common pose estimation methods rely on known 3D object coordinates and 2D image coordinates of reference points. Using reference points provided by markers has multiple advantages for the proposed application of approach manoeuvres: Pose estimates are linked to the charging platform, allowing to determine the relative pose between vehicle and platform. The 3D object coordinates can be obtained, for example by tacheometry, in an Euclidean parking garage coordinate system with metric scale, which could be used as common coordinate system for data fusion with data obtained by other methods (see Section 2.2). Using ArUco markers providing four reference points per marker can increase the robustness in case of partial visibility or bad viewing conditions, as only a single marker has to be detected to make pose estimation possible.

While 3D object coordinates need to be obtained only once, 2D image coordinates of reference points have to be obtained for every acquired image. Consequently, pose estimation using the MB method can be done for every image, in which a sufficient number of markers can be detected. For detecting markers in images and extracting image coordinates of the reference points, there are many methods available in the literature (e.g. GARRIDO-JURADO et al. (2014) for ArUco markers). For estimating vehicle poses, methods solving the perspective-n-point problem (e.g. WU & HU 2006; LEPETIT et al. 2008) can be used, for example.

## 2.2 Markerless vehicle pose estimation ("ML method")

With monocular visual SLAM or structure-from-motion algorithms applied to images taken with the front-looking on-board camera, vehicle poses can be estimated using a sufficient number of image features extracted from images taken during the approach manoeuvre, independent from how many special markers can be detected in these images. As in contrast to the MB method no direct link to the charging platform is given, the vehicle dynamics data $v_{x_i}$ and $v_{y_i}$ describing the

vehicle velocity are derived from two consecutive poses and are fed to the Kalman filter as measurement at time point $t_i$.

E.g. using SLAM or structure-from-motion, a map of 3D points representing the environment in front of the vehicle is created from matches of image features between multiple images. If using a front-looking on-board camera, the created map will cover the environment in the upcoming driveway of the vehicle. Therefore it is likely that later acquired images show parts of the already mapped environment and matches can be obtained for image features between these images and previous ones. By these matches, correspondences between the 3D map points and the later acquired images are established, allowing to use the 3D coordinates of the map points and the 2D image coordinates of the matched features for pose estimation.

With no further information available, the origin, orientation and scale of the map coordinate system are determined by the SLAM or structure-from-motion algorithm and do not correspond with the parking garage coordinate system, wherefore the direct link to the charging platform is not given. For fusing data from the ML method and the MB method, both data should be given in the metric parking garage coordinate system. The metric scale can be obtained for the map coordinate system from a vehicle odometer or being extracted from objects with known size in the environment, like traffic signs (HANEL et al. 2018). The origin and orientation of the map coordinate system can be aligned to the parking garage coordinate system assuming that the vehicle position and driving direction are known at the entry point into the parking garage. As the position of the entry point is prone to large uncertainties (e.g. driveway has multiple lanes), the vehicle velocities $v_{x_i}$ and $v_{y_i}$ and not the vehicle position coordinates $x_i$ and $y_i$ are used as measurement for Kalman filtering.

## 2.3 Mutual vehicle pose estimates using Kalman filtering with vehicle dynamics data obtained from the MB and ML methods

Kalman filtering is applied to obtain mutual vehicle pose estimates in two ways: 1) Pose prediction for time points without any measurements given (time update only), especially if the markers at the charging platform are not visible in the images and 2) pose estimation by fusing vehicle dynamics data provided as measurements by the MB and the ML method (time update and measurement update).

The Kalman state vector contains parameters describing the vehicle dynamics, like planar position or velocity, using special motion models for vehicles, as described by SCHUBERT et al. (2008). Measurement update is done consecutively for different types of measurements (MB, ML) and not in a common update step to be able to perform measurement updates even if not all measurements are available at a time point. A Kalman filter method for non-linear motion models and measurement models is used.

As vehicles typically follow trajectories with multiple straight and curved parts, different motion models might be the most appropriate ones for describing the vehicle dynamics at different time points. Therefore, the motion model used for Kalman filtering should be adaptive: At every time step, all motion models are updated (time update, measurement update) and the motion model providing the best state accuracy is selected, using the state accuracy as the measure for determining the most appropriate model. The steps for model adaption at time point $t_i$ are:

1) State estimates $X_{i,j}$ for all motion models $j$ are calculated from the state estimate in the current motion model using model transfer equations derived from physical relations between the different motion models (e.g. calculating velocity $v_x$ in $x$ direction from total velocity $v$ and vehicle heading angle $\theta$), 2) state covariance matrices $P_{i,j}$ are calculated using error propagation based on the transfer equations and the state covariance matrix of the current motion model, 3) updated state estimates $\hat{X}_{i,j}$ and covariance matrices $\hat{P}_{i,j}$ are obtained either by time update or measurement update for all motion models separately, 4) updated state variances are extracted from $\hat{P}_{i,j}$ and normalized using the state values $\hat{X}_{i,j}$ assuming that larger state values correlate with larger state variances, 5) state accuracy is calculated for each model by averaging the normalized state variances and 6) the motion model for the next Kalman filtering step is adapted to the model with the lowest state accuracy value, the final state $\hat{X}_i$ and covariance matrix $\hat{P}_i$ are given by the state and covariance matrix of this model.

## 3 Simulation of approach manoeuvres to a charging platform

Purpose of the simulation is to compare different motion models, measurements and Kalman filter methods with regard to estimated vehicle poses and their deviation from the ground truth for typical approach manoeuvres to a charging platform.

### 3.1 Simulation settings

In the following, the cases and settings used for simulating approach manoeuvres are described.

**Simulation cases**

The simulation covers the following cases, which are considered as most relevant for the problem addressed in this paper. Additional cases with variations of parameters like the length of the trajectory, the vehicle velocity or the measurement frequency are considered as less relevant.

1) Motion models with the following state parameters describing vehicle dynamics (SCHUBERT et al. 2008): CV ("constant velocity"; position $x_i, y_i$, velocity $v_{x_i}, v_{y_i}$), CTRV ("constant turn rate and velocity"; position $x_i, y_i$, heading angle $\theta_i$, velocity $v_i$, yaw angle $\omega_i$), CTRA ("constant turn rate and acceleration"; position $x_i, y_i$, heading angle $\theta_i$, velocity $v_i$, acceleration $a_i$, yaw angle $\omega_i$), CCA ("constant curvature and acceleration"; position $x_i, y_i$, heading angle $\theta_i$, velocity $v_i$, acceleration $a_i$, curvature $c_i$) and ADAP (the best motion model selected among CV, CTRV, CTRA and CCA for each time point using the approach described in Section 2.3).

2) Measurements: MB (vehicle positions $x_i$ and $y_i$ from marker-based pose estimation), ML (vehicle velocities $v_{x_i}$ and $v_{y_i}$ from markerless pose estimation), CAR (velocity $v_i$ and yaw rate $\omega_i$ from standard vehicle sensors for comparison purpose), MB + ML (combination of $x_i, y_i$ and $v_{x_i}, v_{y_i}$) and MB + ML + CAR (combination of $x_i, y_i$ and $v_{x_i}, v_{y_i}$ and $v_i$ and $\omega_i$).

3) Kalman filter methods: EKF (extended Kalman filter) and UKF (unscented Kalman filter).

4) Approaching manoeuvre trajectories representing typical parking situations: STRAIGHT (driving straight from the driveway into a parking lot at its end) and CURVED (turning right from the driveway into a parking lot on the right side, "transverse parking").

**Trajectories**

The ground truth trajectories (Fig. 3) start at the entry point into the virtual parking garage and end in a parking lot equipped with a charging platform. The charging platform is placed few meters before the end of the trajectory to simulate that markers can't be seen in some images. Both trajectories have the same length of around 30 m.
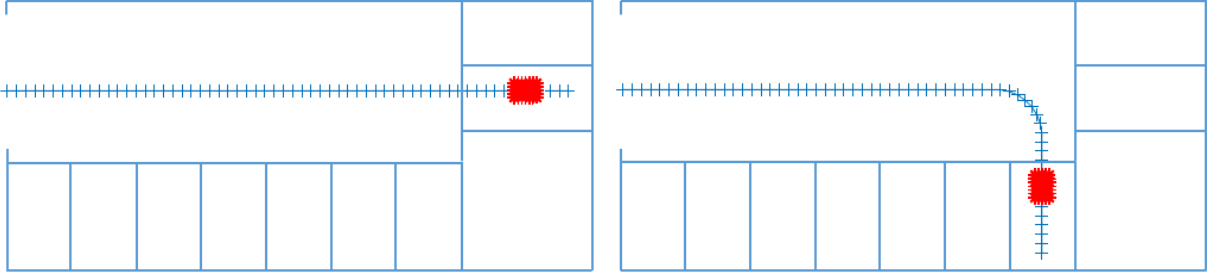


Fig. 3:    Ground floor view of a virtual parking garage with the virtual straight trajectory (left) and curved trajectory (right). The trajectories (blue crossed lines) start at the entry point to the parking garage. The charging platform installed in a parking lot is visualized in red.

The virtual vehicle is moving along the trajectory with a constant velocity of 1 m/s. It is assumed that the dynamics of the virtual vehicle are equal to the virtual front-looking on-board camera.

**Virtual camera**

For specifying the virtual front-looking on-board camera (specifications see Tab. 1), the properties of the front-looking camera used to record the Cityscapes dataset of road scene images (CORDTS et al., 2016) are used.

Tab. 1: Specifications of the virtual camera used for simulation.

| Geometric resolution | 1024 x 2048 px |
|---|---|
| Principal point | 513 px, 1097 px |
| Focal length of the lens | 5 mm |

Tab. 2: Specifications of the virtual markers representing the charging platform.

| Geometry of markers | 7 x 5 grid |
|---|---|
| Distance between markers | 20 cm |
| Marker edge size | 10 cm |
| Reference point distance on a marker | 5 cm |
| Min. marker size in images | 10 px |

**Measurements for Kalman filtering**

Virtual MB measurements $x$ and $y$ are obtained by performing pose estimation (solving the PnP problem) using virtual ArUco markers (specifications see Tab. 2) representing the charging platform. For reference points on the ArUco markers, 3D object coordinates and corresponding 2D image coordinates are simulated. White zero-mean Gaussian noise is added for the sake of realism. Points being far away from the camera tend to lead to large pose errors (PENTENRIEDER et al. 2006), whereas markers which would be imaged with a pixel size below a minimal marker size (threshold see Tab. 2) are not considered for MB measurements. Points which would not be visible in images

(e.g. lying behind the camera) are not considered, as well. Virtual ML measurements $v_x$ and $v_y$ are obtained from position differences between consecutive points along the ground truth trajectory with noise added. ML measurements are not given during ML initialization in the first seven seconds to account for the time needed for correctly initializing scale and orientation (see Section 2.2). Virtual CAR measurements $v$ and $\omega$ are obtained from the ground truth trajectory with noise added. CAR measurements are used for comparison between images as data from additional vehicle sensors and velocity and yaw rate as data from standard vehicle sensors. All virtual measurements are given with a frequency of 2 Hz.

## Kalman filter methods

An extended Kalman filter and an unscented Kalman filter are used as filtering methods. Both methods allow for non-linear motion and measurement models. The extended Kalman filter requires a smaller number of filter parameters to be determined, which might make it more robust to use. In contrast, the unscented Kalman filter does not require Jacobian matrices for time and measurement updates. Therefore, this filter method is not restricted to first-order approximations of the non-linear motion and measurement models, which could lead to sub-optimal performance or sometimes divergence of the extended Kalman filter (WAN & VAN DER MERWE 2000).

## Kalman filter initialization and noise characteristics

For initializing the Kalman filter, the first trajectory position at the entry point into the parking garage is used as initial vehicle position $x_1$, $y_1$ in the parking garage coordinate system. The heading angle $\theta_1$ is set to the trajectory direction at the entry point. The initial velocity $v_1$ is taken from the first CAR measurement, $v_{x_1}$ and $v_{y_1}$ are calculated thereof using $\theta_1$. The initial yaw angle $\omega_1$ is taken from the first CAR measurement, as well, assuming that CAR measurements are available always when the vehicle is in use. As accelerations are not observed by any sensor, $a_1$ is initialized to zero. White zero-mean Gaussian noise is added to all initial values.

The state covariance matrix $P_1$ is initialized with a pessimistic approximation of variance values reported in previous work (e.g. SCHUBERT et al. 2008). A small value of 0.01 is added as covariance between different state parameters taken from the same measurement source (MB, ML, CAR). No covariance is assumed between state parameters from different measurement sources.

Setting process noise covariance matrix $Q$ and measurement noise covariance matrix $R$ for Kalman filtering can be a challenging task (ABBEEL et al. 2005), as often no information about the specific noise characteristics is available. Different strategies for setting those matrices have been proposed (e.g. ODELSON et al. 2006; ÅKESSON et al. 2007). To avoid additional complexity in the simulation, which might correlate with the obtained results, values for $Q$ and $R$ are selected based on assumptions and not on one of the aforementioned strategies. For state parameter variances in $Q$, the same values as for $P_1$ are used. In contrast to $P_1$, the covariance values on the minor diagonals are assumed to be random values obtained from a zero-mean Gaussian distribution with a small sigma of 0.01. Measurement variance values for $R$ are selected based on pessimistic approximation of values reported by PENTENRIEDER et al. (2006), the covariance values assumed to be random values obtained from a zero-mean Gaussian distribution with sigma equal to 0.01. When obtaining the random values for $Q$ and $R$, it is ensured that the symmetry property for covariance matrices is not violated.

## 3.2 Deviation of estimated vehicle positions from the ground truth

The different simulation cases are compared based on the deviation of the estimated mutual vehicle positions from the ground truth positions. The estimates are obtained from 100 executions of each case to avoid biases which might result from specific random values or noise, which are used for the measurements or for initializing the Kalman filter, for example, as described above.

**MB measurements**

For the cases with MB measurements only (Fig. 4), deviations are increasing in the centimetre range as long as measurements are available. When measurements become unavailable (markers not detected anymore → predicted poses, > ~27s), the deviations are increasing in the meter range in only a few seconds. This strong increase can be observed especially for the curved trajectory. A reason for this might be that the prediction begins shortly after the curve in the trajectory, whereas the Kalman filter might not have settled with regard to the new movement direction. Another observation is a stronger increase of the deviation for predicted poses for the UKF than for the EKF.
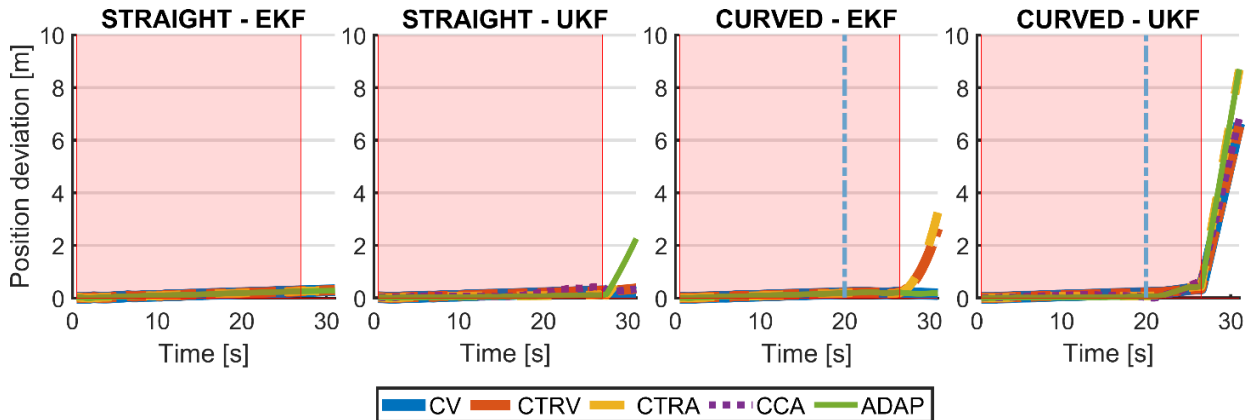


Fig. 4: Position deviation for mutual pose estimates obtained with MB measurements. The vertical dashed line indicates the beginning of the curve in the trajectory. In the beginning of the trajectory (red background color), markers have been available for pose estimation. For later time points (white background) without seeing markers, mutual poses have been predicted only using the Kalman filter.

**ML measurements**

For cases with ML measurements only (Fig. 5), a stronger increase of the deviation can be observed for predicted poses (< ~7 s; time needed for ML initialization) compared to the following time points with measurements available. For the curved trajectory, the deviation increases in a step-like shape at the beginning of the curve (~20 s), which was not observed for the case with MB measurements only. Again, estimates obtained by UKF show larger deviations compared to estimates obtained by EKF.
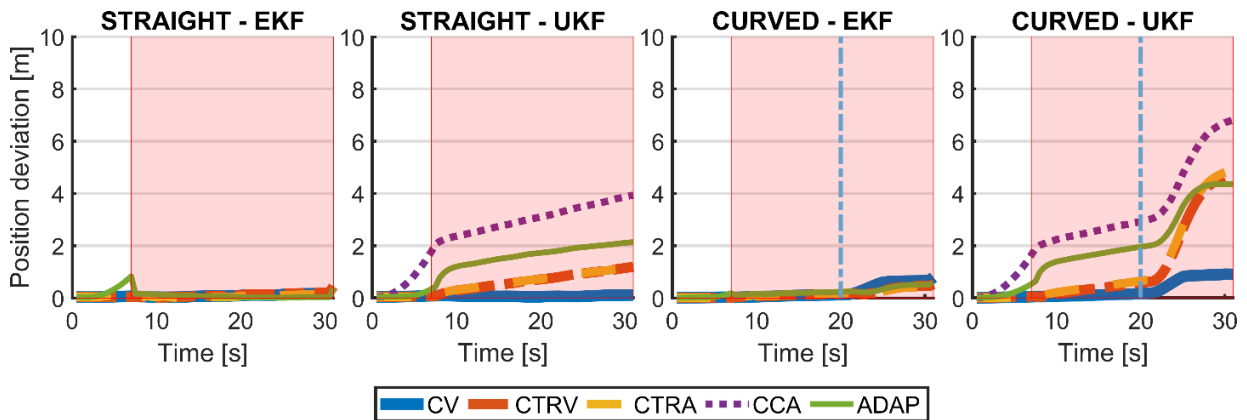
Fig. 5: Position deviation for mutual pose estimates obtained with ML measurements. The vertical dashed line indicates the beginning of the curve in the trajectory. For the first time points (white background color), mutual poses have been predicted only due to the time needed for initializing the ML method. For later time points (red background), measurements have been available.

## CAR measurements

For cases with CAR measurements only (Fig. 6), the motion models CV and ADAP show almost constant strong increase of the deviation of more than one meter per second. A disadvantageous property of the CV model for the given measurements might be that neither the heading angle nor yaw rate are modelled as state parameters. CTRV, CTRA and CCA models having heading angle and yaw rate as state parameters show a remarkably lower increase of the deviation.
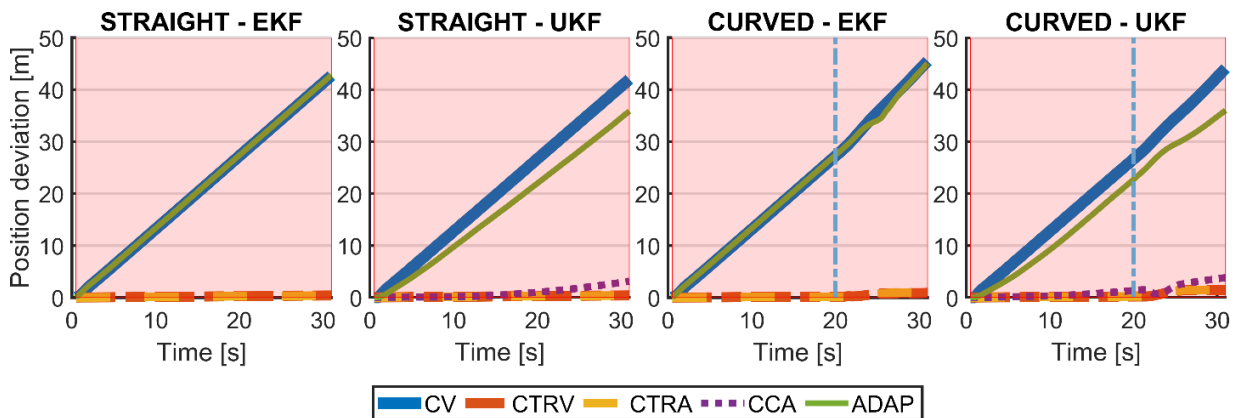


Fig. 6: Position deviation for mutual pose estimates obtained with CAR measurements. The vertical dashed line indicates the beginning of the curve in the trajectory. CAR measurements have been available along the complete trajectory (red background color).

## MB and ML measurements

For cases using MB and ML measurements together (Fig. 7), lower deviation values can be observed at the end of the trajectory (where the charging platform is located) in comparison to cases using MB or ML measurements only. Furthermore, the deviations at the end of the trajectory are similar (max. ~1 m difference) for all of the four cases in Fig. 7 and for all motion models in these cases. The most remarkable increase in the deviation can be observed for the last time points (>

~27 s), for which no MB measurements are available anymore (cf. the red background color in Fig. 4). In contrast to using MB and ML together, for other measurements some of the four cases show remarkably larger deviations than others: Cases with UKF if using MB or ML measurements only, motion models CV and ADAP if using CAR measurements only, for example.
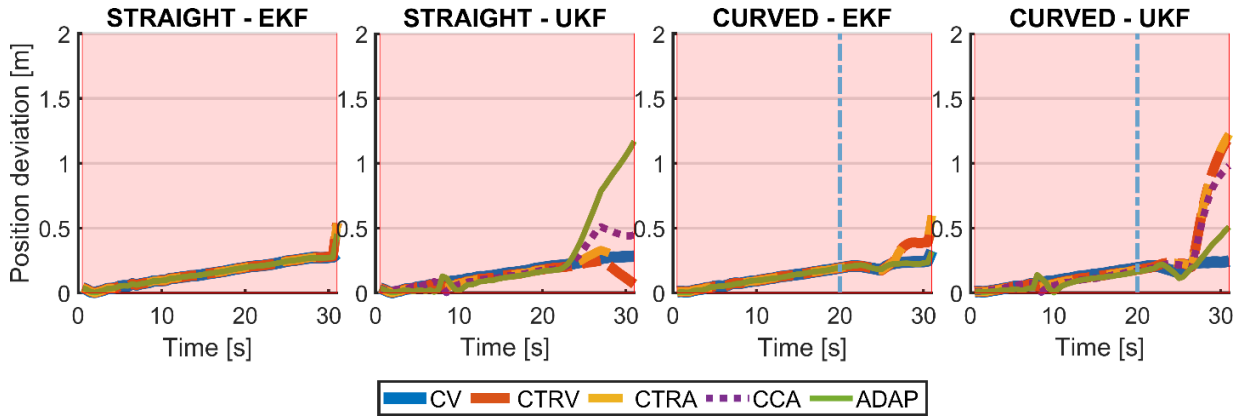


Fig. 7: Position deviation for mutual pose estimates obtained with MB and ML measurements. The vertical dashed line indicates the beginning of the curve in the trajectory. Measurements have been available along the complete trajectory (red background color).

## MB, ML and CAR measurements

For cases using MB, ML and CAR measurements together (Fig. 8), the deviations are larger than for using MB and ML measurements together. In contrast to previous cases for which UKF has shown worse performance, using the EKF shows larger deviations at the end of the trajectory using MB, Ml and CAR measurements. A possible explanation might be that when fusing multiple different types of measurements, the first-order approximation of non-linear motion and measurement models by the EKF might not be sufficient.
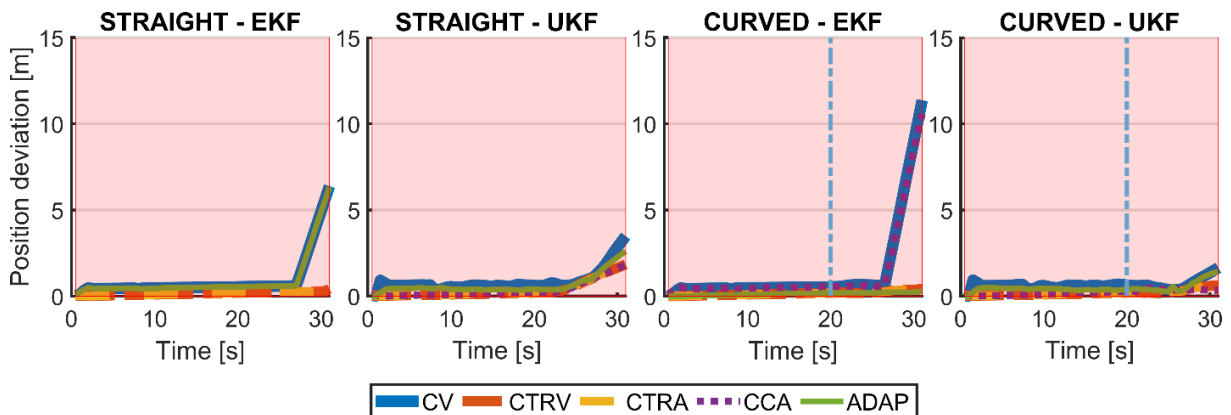


Fig. 8: Position deviation for mutual pose estimates obtained with MB, ML and CAR measurements. The vertical blue dashed line indicates the beginning of the curve in the trajectory. Measurements have been available along the complete trajectory (red background colour).

**General discussion**

For none of the cases it has been analysed whether the deviations are deviations in longitudinal or lateral direction (wrt. the vehicle movement direction). For all cases, the motion model CCA did diverge when using the EKF (deviation values in the range of $10^6$ m and above). As mentioned already in the paragraph above, the first-order approximation of the EKF filter might not be sufficient for this motion model. The adaptive motion model has shown varying performance: For some cases, deviations are lower than for the fixed motion models (CV, CTRV, CTRA, CCA), while for others they are larger. A correlation to simulation settings (like the Kalman method or the trajectory) can't be observed visually. Coming back to the task of aligning an electric vehicle at a charging platform, the results shown above lead to the recommendation to use MB and ML measurements together with EKF. If using MB and ML with EKF, none of the motion models has led to larger deviations than approximately 0.5 m at the end of the trajectory. That avoids the question which motion model to select, which is considered as important for robust application of the proposed method in daily use of vehicles, even though in certain other cases lower deviations (min. ~0.2 m) have been achieved with other measurements. Considering the induced voltage for fine alignment of the vehicle above the charging platform within a maximal misalignment of 0.6 m, a position deviation of approximately 0.5 m can be seen as sufficient for coarse alignment.

## 4  Conclusion

In this paper, a method for vehicle pose estimation relative to a ground-based inductive charging platform represented by special markers has been proposed. In a first step of the method to be performed iteratively during an approach manoeuvre, vehicle dynamics data are independently obtained from camera pose estimation using the markers detected in images acquired by a front-looking on-board camera and from camera pose estimation based on a markerless algorithm like visual SLAM. In a second step, vehicle dynamics data are fused to achieve mutual vehicle pose estimates. By fusing the data from different sources, the proposed method is capable to estimate vehicle poses even if no markers are available, for example because the vehicle is close to the charging platform at the end of the approach manoeuvre. Experiments with simulated camera pose estimates and vehicle dynamics data have shown for typical approach manoeuvers to parking lots that deviations of estimated vehicle positions from the ground truth of around 0.5 m can be achieved using both independent estimations. Obviously, goal of future work could be to test the proposed method in real-world experiments. A further goal could be to test and, if necessary, improve the robustness of the method for bad conditions, which can occur on roads, like rain.

## 5  References

ABBEEL, P., COATES, A., MONTEMERLO, M., NG, A. Y. & THRUN, S., 2005: Discriminative Training of Kalman Filters. Proceedings of Robotics: Science and Systems, **2**, 1.

AICON 3D SYSTEMS GMBH, 2018: ProCam | AICON 3D Systems. Website. https://www.aicon3d.com/en-GB/products/vehicle-testing/procam, last access 2018-10-30.

ÅKESSON, B. M., JØRGENSEN, J. B., POULSEN, N. K. & JØRGENSEN, S. B., 2007: A Tool for Kalman Filter Tuning. Computer Aided Chemical Engineering, **24**, 859-864.

BAY, H., ESS, A., TUYTELAARS, T. & VAN GOOL, L., 2008: Speeded-Up Robust Features (SURF). Computer Vision and Image Understanding, **110**(3), 346-359.

BMWFANS.INFO, 2017: BMW Parts Catalog. Distance Systems, Cruise Control, BMW 750iX G11. http://bmwfans.info/parts-catalog/G11/Europe/750iX-N63R/browse/distance_systems_cruise_control, last access 2017-10-29.

BOMBARDIER TRANSPORTATION, 2013: primove true e-mobility. Brochure. Available online: http://primove.bombardier.com/fileadmin/primove/content/MEDIA/Publications/BT_Brochure_PRIMOVE_210x280_2013_final_upd_110dpi_SP.pdf, last access 2018-12-19.

CORDTS, M., OMRAN, M., RAMOS, S., REHFELD, T., ENZWEILER, M., BENENSON, R., FRANKE, U., ROTH, S. & SCHIELE, B., 2016: The Cityscapes Dataset for Semantic Urban Scene Understanding. IEEE Conference on Computer Vision and Pattern Recognition, 3213-3223.

FITZGIBBON, A. W. & ZISSERMAN, A., 1998: Automatic camera recovery for closed or open image sequences. European Conference on Computer Vision, Springer, 311-326.

GARRIDO-JURADO, S., MUÑOZ-SALINAS, R., MADRID-CUEVAS, F. J. & MARÍN-JIMÉNEZ, M. J., 2014: Automatic generation and detection of highly reliable fiducial markers under occlusion. Pattern Recognition, **47**(6), 2280-2292.

HANEL, A. & STILLA, U., 2017: Calibration of a vehicle camera system with divergent fields-of-view in an urban environment. 37. Wissenschaftlich-Technische Jahrestagung der DGPF, **26**, 160-169.

HANEL A., MITSCHKE, A., BOERNER, R., VAN OPDENBOSCH, D., HOEGNER, L., BRODIE, D. & STILLA, U., 2018: Metric scale calculation for visual mapping algorithms. International Archives of the Photogrammetry, Remote Sensing & Spatial Information Sciences, XLII-2, 433-440.

HWANG, K., CHO, J., PARK, J., KIM, D., KWON, J.H., KWAK, S.I., PARK, H.H. & AHN, S., 2016: An Autonomous Steering System for Wireless Charging Electric Vehicles to Minimize Power Degradation. 2016 3rd Asia-Pacific World Congress on Computer Science and Engineeringha, 60-65.

LEMAIRE, T., BERGER, C., JUNG, I.-K. & LACROIX, S., 2007: Vision-Based SLAM: Stereo and Monocular Approaches. International Journal of Computer Vision, **74**(3), 343-364.

LEPETIT, V., MORENO-NOGUER, F. & FUA, P., 2008: EPnP: An Accurate O(n) Solution to the PnP Problem. International Journal of Computer Vision, **81**, 155-166.

LOWE, D. G., 1999: Object recognition from local scale-invariant features. Proceedings of the Seventh IEEE International Conference on Computer Vision, **2**, 1150-1157.

NAIMARK, L. & FOXLIN, E., 2002: Circular data matrix fiducial system and robust image processing for a wearable vision-inertial self-tracker. Proceedings of the International Symposium on Mixed and Augmented Reality, 27-36.

NISTER, D., NARODITSKY, O. & BERGEN, J., 2004: Visual odometry. Proceedings of the IEEE 2004 Computer Society Conference on Computer Vision and Pattern Recognition, **1**, I-652-I-659.

ODELSON, B. J., RAJAMANI, M. R. & RAWLINGS, J. B., 2006: A new autocovariance least-squares method for estimating noise covariances. Automatica, **42**(2), 303-308.

PANCHAL, C., STEGEN, S. & LU, J., 2018: Review of static and dynamic wireless electric vehicle charging system. Engineering Science and Technology, **21**(5), 922-937.

PENTENRIEDER, K., MEIER, P. & KLINKER, G., 2006: Analysis of Tracking Accuracy for Single-Camera Square-Marker-Based Tracking. Proceedings of Dritter Workshop "Virtuelle und Erweiterte Realität der GI-Fachgruppe VR/AR".

ROMERO RAMIREZ, F. J., MUÑOZ-SALINAS, R. & MEDINA-CARNICER, R., 2018: Speeded Up Detection of Squared Fiducial Markers. Image and Vision Computing, **76**, 38-47.

RUBLEE, E., RABAUD, V., KONOLIGE, K. & BRADSKI, G., 2011: ORB: An Efficient Alternative to SIFT or SURF. Proceedings of the 2011 International Conference on Computer Vision, 2564-2571.

SCHUBERT, R., RICHTER, E. & WANIELIK, G., 2008: Comparison and Evaluation of Advanced Motion Models for Vehicle Tracking. 11th International Conference on Information Fusion, 730-735.

SHAO, S., GUO, S. & QIU, X., 2017: A Mobile Battery Swapping Service for Electric Vehicles Based on a Battery Swapping Van. Energies 2017, **10**, article number 1667.

WAN, E. A. & VAN DER MERWE, R., 2000: The Unscented Kalman Filter for Nonlinear Estimation. Proceedins oft he IEEE 2000 Adaptive Systems for Signal Processing, Communications, and Control Symposium, 153-158.

WU, Y. & HU, Z., 2006: PnP Problem Revisited. Journal of Mathematical Imaging and Vision, **24**, 131-141.

ZIEBINSKI, A., CUPEK, R., ERDOGAN, H. & WAECHTER, S., 2016: A Survey of ADAS Technologies for the Future Perspective of Sensor Fusion. Computational Collective Intelligence, 135-146.